A Revised Bourgouin Precipitation-Type Algorithm

KEVIN BIRK,[a] ERIC LENNING,[a] KEVIN DONOFRIO,[a] AND MATTHEW T. FRIEDLEIN[a]

[a] *National Oceanic and Atmospheric Administration, National Weather Service, Romeoville, Illinois*

(Manuscript received 14 July 2020, in final form 24 December 2020)

ABSTRACT: Using vertical temperature profiles obtained from upper-air observations or numerical weather prediction models, the Bourgouin technique calculates areas of positive melting energy and negative refreezing energy for determining precipitation type. Energies are proportional to the product of the mean temperature of a layer and its depth. Layers warmer than 0°C consist of positive energy; those colder than 0°C consist of negative energy. Sufficient melting or freezing energy in a layer can produce a phase change in a falling hydrometeor. The Bourgouin technique utilizes these energies to determine the likelihood of rain (RA) versus snow (SN) given a surface-based melting layer and ice pellets (PL) versus freezing rain (FZRA) or RA given an elevated melting layer. The Bourgouin approach was developed from a relatively small dataset but has been widely utilized by operational forecasters and in postprocessing of NWP output. Recent analysis with a larger dataset suggests ways to improve the original technique, especially when discriminating PL from FZRA or RA. This and several other issues are addressed by a modified version of the Bourgouin technique described in this article. Additional enhancements include use of the wet-bulb profile rather than temperature, a check for heterogeneous ice nucleation, and output that includes probabilities of four different weather types (RA, SN, FZRA, PL) rather than the single most likely type. Together these revisions result in improved performance and provide a more viable and valuable tool for precipitation-type forecasts. Several National Weather Service forecast offices have successfully utilized the revised tool in recent winters.

SIGNIFICANCE STATEMENT: This article describes an updated version of a widely used technique for predicting winter precipitation type at the surface. Verification statistics suggest the revised technique outperforms the original version. It also compares favorably to a more sophisticated approach for postprocessing of model output yet is simple enough for operational meteorologists to use for making real-time, critical forecast adjustments. This updated technique was adapted as the basis for precipitation-type forecasts in the NWS National Blend of Models starting with version 3.2. It also is the approach that several NWS offices have adapted for their winter forecasts in recent years. Future efforts should seek to further refine this technique and make greater use of its inherent probabilistic information.

KEYWORDS: Forecast verification/skill; Forecasting; Forecasting techniques; Operational forecasting; Probability forecasts/models/distribution; Mixed precipitation; Freezing precipitation; Winter/cool season

1. Introduction

Determination of winter precipitation type is a significant forecast challenge (Ralph et al. 2005), especially in thermal environments where rain (RA), snow (SN), freezing rain (FZRA), or ice pellets in the form of sleet (PL) all may be possible. Impacts to society and the economy from different precipitation types also can vary significantly. For example, a few millimeters of liquid-equivalent precipitation in the form of FZRA could produce much greater impacts than this same amount falling as RA, SN, or PL (Changnon 2003).

This challenge is compounded by increasing demands for high temporal and spatial resolution gridded forecasts. The NWS provides much of its forecast information through the National Digital Forecast Database (NDFD; Glahn and Ruth 2003). The NDFD offers forecasts of sensible weather elements (e.g., cloud cover, temperature, precipitation type) on a horizontal grid of 2.5-km resolution, often in hourly increments. The database is populated and regularly updated by meteorologists at local NWS offices around the country so that it reflects current observational trends as well as the most likely forecast scenario. The portion of the NDFD maintained by each office contains thousands of grid points.

At longer time ranges NWS meteorologists rely primarily on numerical weather prediction models to guide their forecast decisions. At close time ranges observational datasets play a larger role. In both cases, deviations from model guidance often are necessary, though interelement consistency within the NDFD must be maintained. For example, if hourly temperatures at certain grid points are adjusted from above freezing to below, the precipitation types and accumulations also must change for those hours and grid points. In fact, managing the hourly evolution of precipitation type across thousands of 2.5-km grids is one of the more challenging tasks an NWS forecaster faces.

The frequent need to adjust away from model guidance also is what motivates the use of implicit techniques based on vertical thermal profiles rather than explicit techniques utilizing model microphysics. Reeves et al. (2016) discusses a number of limitations related to model microphysics schemes. One not mentioned is that when a model is struggling to match surface and upper-air observational trends, explicit precipitation-type output based on its microphysics will misrepresent what is actually occurring at a particular time and location. Tools for

Corresponding author: Kevin Birk, kevin.birk@noaa.gov

DOI: 10.1175/WAF-D-20-0118.1

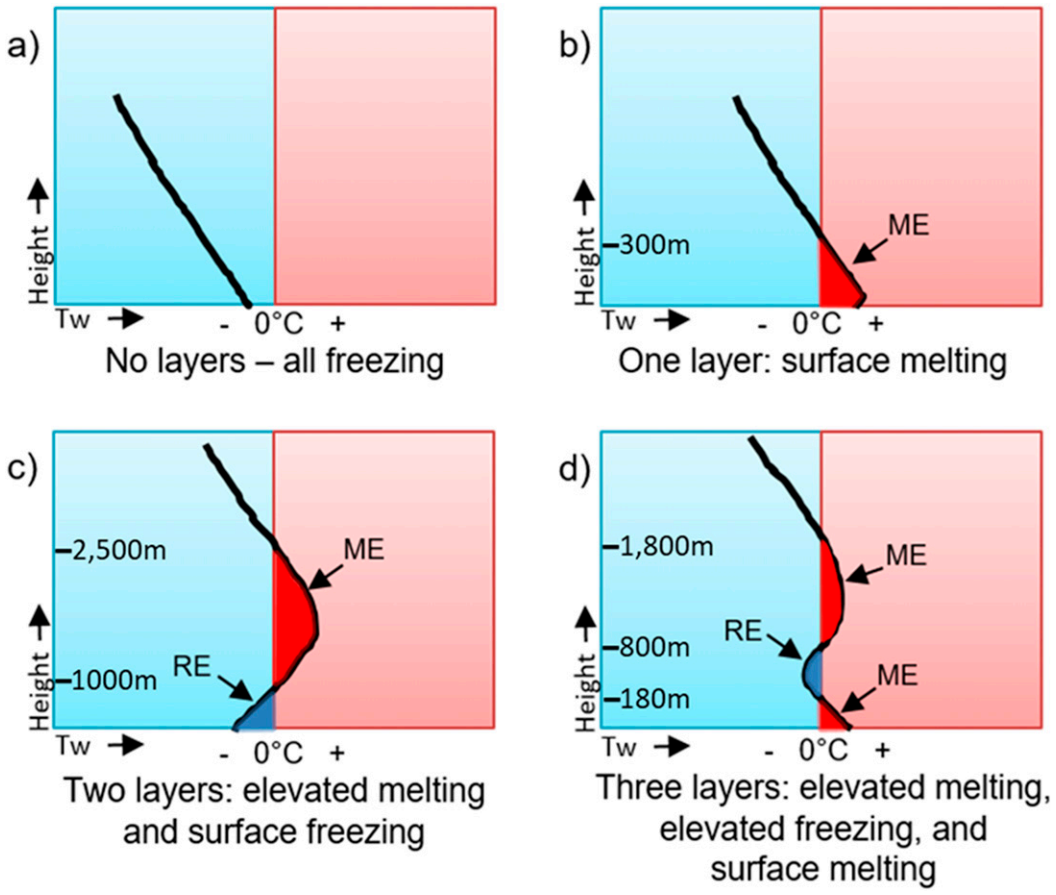

FIG. 1. Wet-bulb temperature T_w profiles typically associated with (a) SN; (b) RA and/or SN; (c) FZRA and/or PL and/or SN; and (d) as in (c), but with RA instead of FZRA. Layers of melting energy (ME) and refreezing energy (RE) also are shown. Example heights along the y axis are representative values, but in the real world there are no limits on how these may vary.

making real-time forecast adjustments rely on the latest observations and do not have access to the internal microphysics of a model.

This paper describes a simple but effective implicit technique to assist in the operational forecasting of precipitation type. This is based on a revised version of the Bourgouin (2000) area method, referred to here as the Modified Bourgouin method. Section 2 describes three precipitation-type algorithms: the spectral bin classifier (Reeves et al. 2016), the traditional top-down approach used by many NWS offices (Baumgardt 2000), and the original Bourgouin area method. Section 3 explores motivations for a revised version of the Bourgouin approach. Section 4 describes the development of this revised algorithm. Section 5 shows how the revised technique performs relative to the other three. Section 6 provides a discussion and conclusions.

2. Precipitation-type algorithms for operational forecasts

a. Precipitation-type environments

Precipitation-type forecasts consider two key questions: whether there will be ice nucleation and whether there will be phase changes before hydrometeors reach the surface. The temperature profile in the lower troposphere can play a large role in determining the phase change potential (Czys et al. 1996) though the wet-bulb temperature T_w profile can be even more important (Ramer 1993; Baldwin et al. 1994; Schuur et al. 2012; Reeves et al. 2016) likely because T_w is more representative of the temperature experienced by particles large enough to survive evaporation.

Figure 1 summarizes four basic scenarios that can evolve when ice nucleation does occur. In the simplest case (Fig. 1a) the entire vertical profile is below freezing which supports SN. With a surface-based melting layer (layer with T_w above 0°C, Fig. 1b) the outcome is RA and/or SN depending on the depth and magnitude of that layer. An elevated melting layer (Fig. 1c) supports SN, FZRA, PL, or mixtures of all three. With another melting layer at the surface (Fig. 1d), RA replaces FZRA.

In addition to the temperature or wet-bulb profile, hydrometeor sizes also can affect whether a phase change occurs (Crawford and Stewart 1995; Bernstein 2000; Cortinas 2000; Rauber et al. 2000, 2001; Robbins and Cortinas 2002; Changnon 2003; Cortinas et al. 2004; Thériault et al. 2010).

In real time the hydrometeor size distribution is difficult to account for given the lack of sampling and thus is neglected in many precipitation type methods.

b. The spectral bin classifier

One algorithm that does account for hydrometeor size and has been shown to outperform other common implicit methods is the spectral bin classifier (SBC; Reeves et al. 2016). The SBC first considers the potential for ice nucleation then calculates melting and refreezing rates for hydrometeors of various sizes as they fall. It chooses one most likely precipitation type out of six possible categories: SN, RA, FZRA, PL, RASN, and FZRAPL. It does not provide information regarding the relative probability of alternate types.

While the SBC explicitly accounts for hydrometeor size during melting and refreezing, size is not considered during the initial determination of ice nucleation. Of note, the spectrum of hydrometeor sizes used by the algorithm is based on a static and theoretical distribution of drop sizes, not one determined uniquely for each situation. Additionally, the algorithm requires a detailed vertical temperature or wet-bulb profile. On the 2.5-km NDFD grid it would be difficult to adjust in real time a complete profile at each point. This algorithm therefore may be more suited to postprocessing of NWP output than manipulation by operational forecasters. Its skill relative to other approaches warrants inclusion in this discussion for comparison purposes.

c. The traditional top-down approach

A simpler approach to diagnosing phase change potential in a layer is to consider only one temperature variable: the maximum temperature or wet bulb in the melting layer, and the minimum temperature or wet bulb in the refreezing layer. This is the traditional top-down approach used in many NWS offices (Baumgardt 2000). As with the SBC, this also considers the potential for ice nucleation. Unlike the SBC it does not directly account for hydrometeor size. It does allow for certain combinations of mixed events by providing information regarding the relative probability of multiple precipitation types (RA, SN, FZRA, and PL) rather than trying to determine a single most likely outcome.

The traditional top-down approach works well for many scenarios. A key exception would be situations with isothermal layers in which the maximum or minimum temperature is less representative of the total melting or refreezing potential.

d. The Bourgouin method

Starting in 2016, some NWS offices have utilized an approach adapted from Bourgouin (2000). This improves over the traditional top-down method by accounting for both the depth and magnitude of a temperature layer, thus properly calculating the true melting or refreezing potential even in isothermal layers.

As with the traditional top-down approach, the Bourgouin technique requires a forecaster to manipulate only two variables (melting and refreezing energy) to adjust melting and refreezing potential. The advantage is that these variables more accurately reflect the phase change potential within a layer. And while the initial computation of energy values requires a detailed vertical profile, the use of simple layer-summary parameters facilitates subsequent real-time adjustments by the forecaster and calculations by the algorithm.

The next section describes the original Bourgouin approach in greater detail while also explaining several motivations for an enhanced version of this technique. Section 4 then describes the process utilized to develop this enhanced version.

3. Addressing limitations of the original Bourgouin area method

Since its introduction, the Bourgouin technique has been widely utilized by operational meteorologists via the BUFKIT program for examining forecast soundings (Mahoney and Niziol 1997) and in postprocessing of NWP output (Mullens and McPherson 2017; Wandishin et al. 2005). This technique is one of several algorithms Manikin (2005) combined into a single predominant precipitation-type value for use at NCEP (http://www.wpc.ncep.noaa.gov/wwd/impactgraphics/). Even so, the original version has a number of limitations that hinder its effectiveness. Some of these were discovered through the use of this tool for operational forecasts. Others were identified in a previous evaluation (Reeves et al. 2014) or anticipated in the paper which introduced this technique (Bourgouin 2000). The following discussion summarizes the original approach and explains motivations for a revised version of the algorithm.

a. The original Bourgouin area method

The area method assumes that a phase change of a falling hydrometeor in a melting (or warm, above 0°C) or refreezing (or cold, below 0°C) layer is driven by the depth and average temperature of that layer, the product of which is proportional to areas on a thermodynamic diagram (Bourgouin 2000). This provides an easy way to evaluate the negative/refreezing or positive/melting area in terms of energy (J kg^{-1}):

$$\text{energy area} = \int_{z_l}^{z_u} g\left(\frac{T_{\text{env}} - T_0}{T_0}\right) dz\,. \tag{1}$$

When integrating across an entire melting or freezing layer, z_u would always be a freezing level and z_l would be the next lower freezing level or, for a surface-based freezing or melting layer, the surface. Here, T_0 is 273.15 K, and T_{env} is the environmental temperature in kelvin at a given level. The result of Eq. (1) thus is negative for subfreezing layers. However, for the purposes of this paper both positive/melting and negative/refreezing areas are expressed as positive values.

Using this approach, a sounding with no positive energy is classified as SN. If the only melting layer (defined as having at least 2 J kg^{-1} of positive energy) is surface based, the prediction is RA and/or SN depending on the magnitude of positive energy in that layer. With an elevated melting layer and surface-based refreezing layer the options are FZRA and/or PL depending on the ratio of melting and refreezing energy in the two layers. An additional surface melting layer would yield RA in place of FZRA.

TABLE 1. Cases for each precipitation type in the present study.

Precipitation type	Developmental dataset	Independent dataset
FZRA	124	100
PL	28	14
SNPL	13	23
FZRAPL	53	16
FZRAPLSN	24	19
Total	242	172

b. Probability of mixed events

Like the SBC, the original Bourgouin approach chooses one most likely precipitation type out of six possible categories (SN, RA, FZRA, PL, RASN, and FZRAPL). Since information regarding the most likely alternatives would be of value operationally, the Modified Bourgouin approach always predicts the probability of all four basic types (RA, SN, FZRA, and PL). This allows for all varieties of wintry mixes (e.g., SNPL, FZRAPL, and FZRAPLSN) and gives information about the relative contribution from each basic type.

This probability of weather type (PoWT) approach also addresses other inherent uncertainties, either from NWP models or observed soundings. Even over a 2.5-km grid box and the span of 60 min, as forecasts are represented in the NDFD, there can be variations in the vertical thermal profile and thus in observed precipitation types. The PoWT approach offers insights regarding the most likely variations across space and time. In this way it also is more forgiving of observation or model errors, though like any technique will begin to fail as these errors become more egregious.

c. Developmental and independent datasets

The Bourgouin technique is a perfect-prog approach (Klein et al. 1959) derived from a database of surface observations and upper-air soundings. One factor acknowledged as potentially limiting the effectiveness of the original version is its relatively small developmental dataset. To establish thresholds separating FZRA from PL, the study utilized just 20 observations of PL, 31 of FZRA, and 3 of a mix. For distinguishing RA and SN the situation was somewhat better, with 53 observations of SN, 51 of RA, and 15 of a mix. The independent dataset for evaluation of the technique relative to other methods was even smaller.

To reassess these thresholds, a larger dataset is used. Our developmental dataset consists of 242 winter precipitation events across North America prior to 2006 (Table 1). To be used in the study, the reported precipitation event had to occur within a 35 km radius and within ±1 h of the time of a radiosonde observation, and surface observations had to be from locations with a human observer to ensure PL could be correctly detected (Landolt et al. 2019). Observations from Reeves et al. (2014) spanning the years 2002–05 were included in this dataset after an additional round of quality control. Many of the cases are from the mid-1980s through the 1990s, with a few dating back to the late 1970s.

An independent dataset for this new study is compiled from the years 2006–19. This includes the Reeves et al. (2014) events from 2006 to 2013. In total, there are 172 winter precipitation cases across North America in the new independent dataset (Table 1).

d. Temperature versus wet-bulb temperature

While the original Bourgouin method uses the vertical temperature profile for the calculation of layer energy, the revised version uses the T_w profile which likely offers a better discriminator (Ramer 1993; Baldwin et al. 1994; Schuur et al. 2012; Reeves et al. 2016) as previously discussed. Positive and negative T_w energy areas can be computed by substituting the environmental wet-bulb temperature ($T_{w\text{-env}}$) in place of T_{env} in Eq. (1). This provides for the possibility of phase changes due to evaporative cooling in unsaturated layers.

e. Ice nucleation

The original Bourgouin method does not diagnose freezing drizzle, yet in Figs. 1a and 1c this or freezing rain is the most likely outcome if ice nucleation does not occur. Several studies have found that the activation of ice nuclei increases as cloud top temperatures drop through the range from −8° to −15°C (Rasmussen et al. 2002; Schichtel 1988; Politovich 1996; Pobanz et al. 1994; Bernstein 2000).

Given the importance of correctly identifying cases of freezing precipitation as a result of warmer clouds lacking ice nucleation, the Modified Bourgouin method includes the same probability of ice present (ProbIce) calculation used by the traditional top-down method (Baumgardt et al. 2017). This assumes layers of a sounding are saturated and capable of generating precipitation when they exceed 1 km in depth and have relative humidity with respect to ice (RH_{Ice}) greater than 75%. It then assigns a ProbIce percentage based on the minimum temperature in such a layer using these rules as shown in Fig. 2:

$$\text{If} \quad T \le -15^\circ\text{C}, \text{ then ProbIce} = 100\%, \tag{2a}$$

$$\text{If} \quad -15^\circ\text{C} < T < -7^\circ\text{C}, \text{ then}$$

$$\text{ProbIce} = -0.065T^4 - 3.1544T^3 - 56.414T^2 - 449.6T - 1308, \tag{2b}$$

$$\text{If} \quad T \ge -7^\circ\text{C}, \text{ then ProbIce} = 0\%, \tag{2c}$$

where T is the temperature in degrees Celsius. If a precipitation generation layer exists above a dry layer with $\text{RH}_{\text{Ice}} <$ 75% for more than 1500 m, sublimation is assumed, and this upper layer is eliminated from consideration.

f. Hydrometeor size

Unlike the SBC, neither the original nor the Modified Bourgouin approach directly considers hydrometeor size in any of its calculations. However, the revised technique does so indirectly by assuming there is a spectrum of hydrometeors in any winter precipitation scenario and that larger hydrometeors require more energy to prompt a complete phase change (Zerr 1997). Thus with increasing amounts of positive (negative) energy, the chance is greater that all hydrometeors will melt (refreeze).

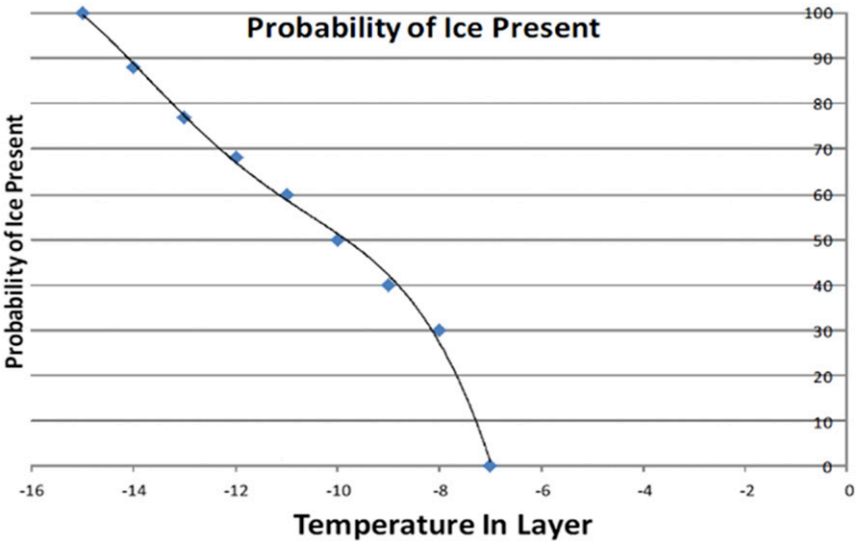

FIG. 2. Probability of heterogeneous ice nucleation in a precipitation generation layer. Reproduced from Baumgardt et al. (2017).

4. Development of the Modified Bourgouin technique

The Modified Bourgouin technique as outlined above has several improvements over the original:

- a larger developmental and independent dataset;
- use of wet-bulb temperature profiles;
- ability to diagnose freezing precipitation in situations without ice nucleation;
- probabilistic output that accounts for uncertainties in the spectrum of hydrometeor sizes, forecast or observed soundings, and space and time, and
- allowance for all combinations of wintry mixes.

With these enhancements, there are two key issues that require greater scrutiny: a new threshold for delineating FZRA or RA from PL, and a method for determining when to include SN even with an elevated melting layer.

a. Criteria for FZRA or RA and PL

A key limitation of the relatively small Bourgouin (2000) developmental dataset is the lack of PL and FZRA cases with large values of positive energy. This is especially true for PL events, with only one having more than 150 J kg^{-1}. For this technique, the basic question is how much energy is required to produce a phase change. A related question for PL and FZRA is whether the magnitude of positive energy in the elevated melting layer influences the amount of negative energy needed to refreeze a hydrometeor. The original study suggests a completely melted hydrometeor requires considerably more negative energy to refreeze when there is a larger amount of positive energy. However, given the limited range of positive energy in the original dataset, this question is worth revisiting using a larger number of cases.

Figure 3 shows all cases in the new developmental dataset with FZRA and/or PL. Since the goal here is to determine thresholds between different precipitation types based off the T_w profile, only cases with at least an 80% chance of heterogeneous ice nucleation were included in the figure. This figure, similar to Fig. 2 from Bourgouin (2000), plots all events as a function of the positive/melting and negative/refreezing energies. However, energies here are based on T_w profiles. For reference the yellow line shows the original Bourgouin FZRA versus PL threshold.

There is some overlap of cases as in the original Bourgouin study, including a zone where FZRA and PL events appear equally likely, though pure FZRA events become less favored as negative energy values increase. The goal is to find a function that best separates pure FZRA events from those containing PL, either as part of a wintry mix or as the sole precipitation type. Using a two-category, two-dimensional linear discriminant analysis to classify members of the dataset, this function was identified as follows:

$$\mathrm{RE_{Tw}} = 117 + 0.08\mathrm{ME_{Tw}}, \tag{3}$$

where $\mathrm{RE_{Tw}}$ represents the wet-bulb refreezing energy (J kg^{-1}) and $\mathrm{ME_{Tw}}$ is the wet-bulb melting energy. It is worth noting that this reflects a smaller dependence on melting energy magnitudes than in the original technique. This either implies there is little warming of the liquid water droplet from additional $\mathrm{ME_{Tw}}$, or that this warming has only a small effect on whether the hydrometeor will refreeze.

Equation (3) offers a reasonable separation between pure FZRA cases and those that include PL, especially for cases in which total melting of all hydrometeors is occurring. However, a closer examination of Fig. 3 suggests the threshold between pure FZRA events and those containing PL becomes much more dependent on the magnitude of the melting energy for cases possessing weak warm layers that only support partially melted hydrometeors. Further analysis on mixed precipitation type cases that were misclassified using Eq. (3) indicated that a majority of these cases occurred when melting

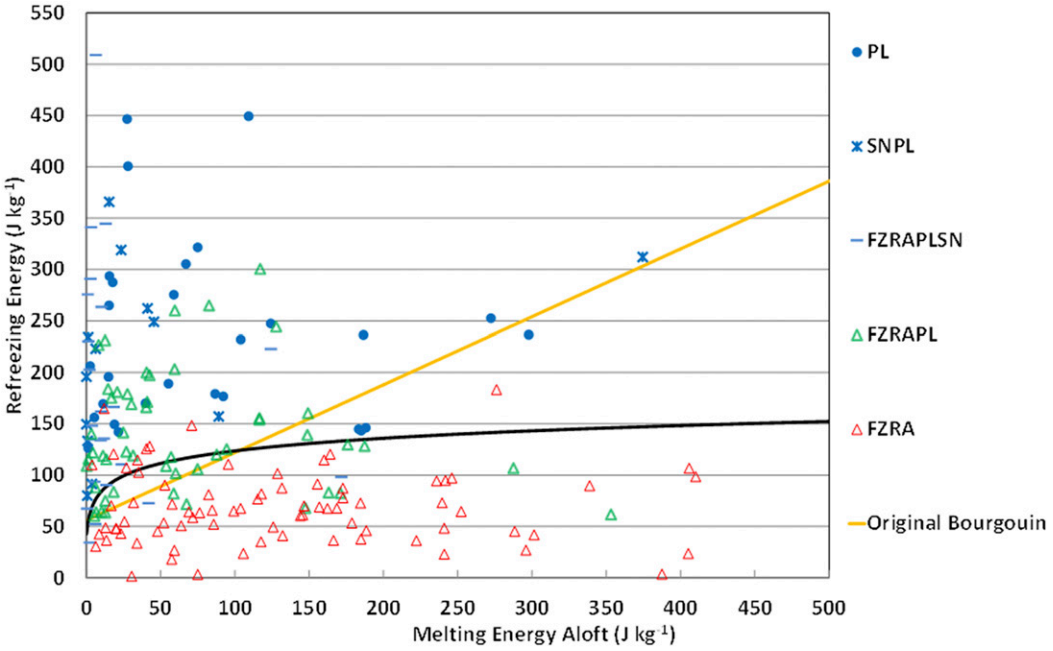

FIG. 3. Observations in the developmental dataset as a function of melting and refreezing wet-bulb energy. The yellow line is the Bourgouin (2000) function to separate FZRA from PL. The black line is the new threshold between pure FZRA and mixes containing PL.

energies were less than 30 J kg^{-1}. Therefore, the data suggest that as melting energies drop below 30 J kg^{-1}, it becomes increasingly likely that some hydrometeors maintain a frozen nucleus. This aligns with previous studies, including Reeves et al. (2016), which also found that partially melted hydrometeors more readily refreeze to PL. A separate function to discriminate pure FZRA events from those also containing PL was investigated for these partial melting cases and through linear discriminant analysis was found to be

$$\mathrm{RE_{Tw}} = 31.4 + 2.9\mathrm{ME_{Tw}}. \tag{4}$$

As a final step, a logarithmic function was fit to Eqs. (3) and (4), thus making our final function used to differentiate pure FZRA events from those that include PL as follows:

$$\mathrm{RE_{Tw}} = 41 + 17.9\ln(\mathrm{ME_{Tw}} + 1). \tag{5}$$

Note that 1 is added to the $\mathrm{ME_{Tw}}$ to ensure that $\mathrm{RE_{Tw}}$ does not go negative as the $\mathrm{ME_{Tw}}$ approaches zero. This line is illustrated in Fig. 3.

Figure 4 shows distributions of elevated $\mathrm{ME_{Tw}}$ along with the surface layer $\mathrm{RE_{Tw}}$ for FZRA, PL, and mixed events from the developmental dataset. While there is considerable overlap in $\mathrm{ME_{Tw}}$ magnitudes for these events, there is little to no overlap in $\mathrm{RE_{Tw}}$ magnitudes between the two pure precipitation types. Pure FZRA events also have significantly less $\mathrm{RE_{Tw}}$ than events containing any PL. Therefore, $\mathrm{RE_{Tw}}$ is the most important predictor for the occurrence of PL once the hydrometeor is totally melted.

While Eq. (5) represents the primary separation between pure FZRA events and those with at least some PL, it also is helpful to identify zones where one is more likely or both are equally likely. Equation (6) describes these zones, which also are illustrated in Fig. 5:

$$\text{FZRA dominant: } \mathrm{RE_{Tw}} < 41 + 17.9\ln(\mathrm{ME_{Tw}} + 1), \tag{6a}$$

$$\text{Equal chances PL and FZRA: } 41 + 17.9\ln(\mathrm{ME_{Tw}} + 1) \le \mathrm{RE_{Tw}} \le 170 + 0.08\mathrm{ME_{Tw}}, \tag{6b}$$

$$\text{PL dominant: } \mathrm{RE_{Tw}} > 170 + 0.08\mathrm{ME_{Tw}}. \tag{6c}$$

While the lower threshold [Eq. (6a)] is simply our derived logarithmic function from Eq. (5), the upper threshold defined here represents the point at which the chances of having an event of pure PL exceeds that of one mixed with FZRA. The $\mathrm{RE_{Tw}}$ of 170 J kg^{-1} in Eq. (6c) represents the distribution crossing of the highest 30th percentile of mixed FZRA events and the lowest 30th percentile of pure PL events. Since this transition does not appear to follow a logarithmic function, we use a linear threshold with the same slope as defined in Eq. (3) above. This threshold also provided the best verification using the developmental dataset.

Since Eqs. (5) and (6) do not correctly classify every event deterministically, the use of probabilities can improve this. In the zone of equal chances shown in Eq. (6b) we define the probabilities of FZRA and PL to both be 100%. Above and below this zone, the probabilities of the less favored type linearly decrease from 100% to below 20%. The threshold above which cases containing FZRA in the observation dropped below 20% was when $\mathrm{RE_{Tw}} > 208 + 0.08\mathrm{ME_{Tw}}$, where

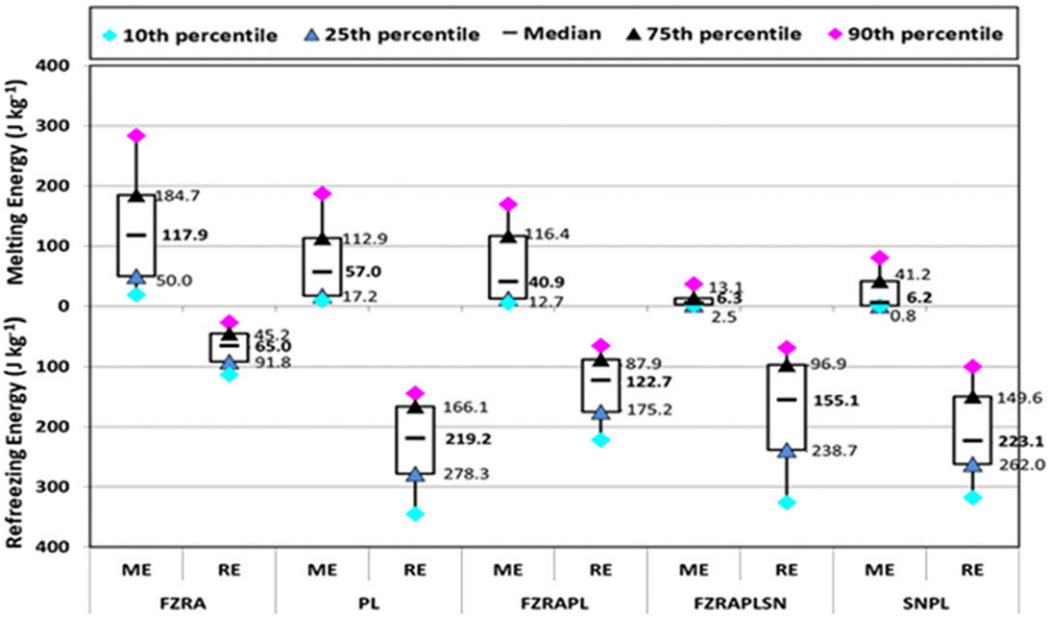

FIG. 4. Wet-bulb melting and refreezing energy (ME and RE) for each precipitation type in the developmental dataset.

208 J kg^{-1} is approximately the 80th percentile of the RE_{Tw} from the distribution of wintry mixes containing FZRA. A linear best fit function that dropped the probabilitiy of FZRA (ProbFZRA) in this matter was found to be

$$\text{ProbFZRA} = -2.1\text{RE}_{\text{Tw}} + 0.2\text{ME}_{\text{Tw}} + 458, \qquad (7)$$

with results constrained to values between 0 and 100. ProbFZRA becomes ProbRA, when the surface $T_w > 0$°C.

For FZRA, situations with barely any positive energy require special attention. In these cases PL and SN become increasingly favored, either because hydrometeors are only partially melted and thus easier to refreeze (Czys et al. 1996; Rauber et al. 2001; Reeves et al. 2016) or because hydrometeors experience little melting at all. To avoid over forecasting FZRA, the result from Eq. (7) is multiplied by 20% of the ME_{Tw} when melting energy is <5 J kg^{-1} (approximately the 10th percentile of ME_{Tw} for cases with FZRA). This is

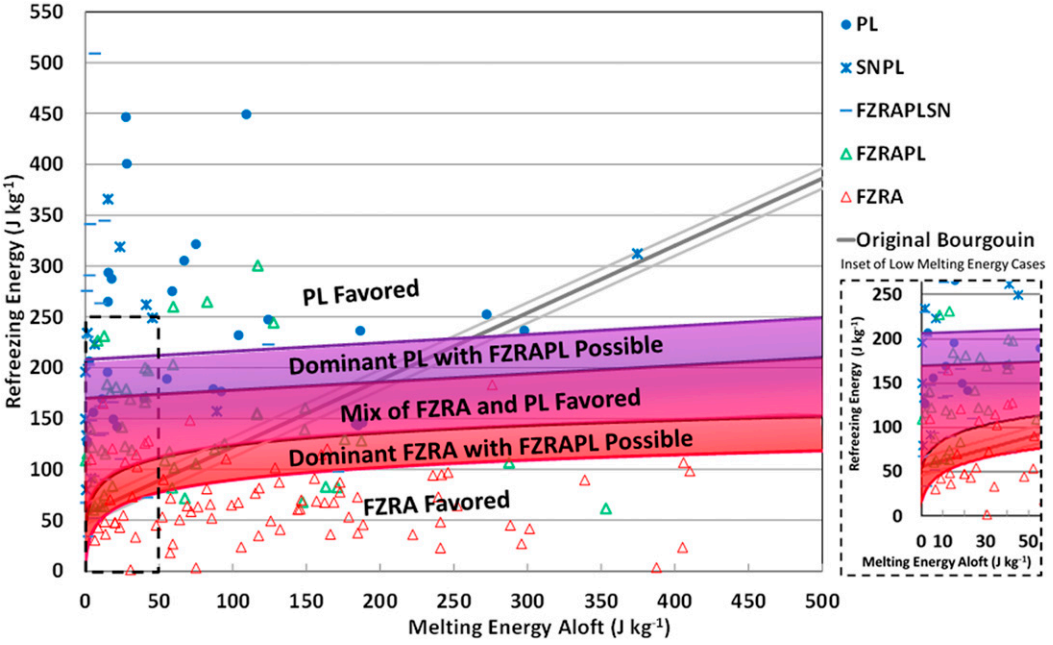

FIG. 5. As in Fig. 3,. The shaded transition zones are used probabilistically to discriminate between FZRA and PL.

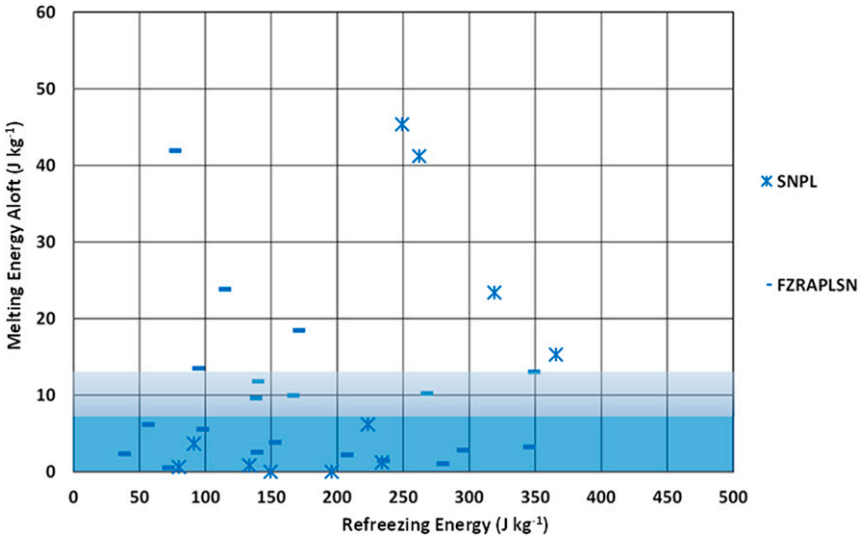

FIG. 6. Mixed precipitation cases including SN as a function of melting and refreezing wet-bulb energies (ME_{Tw} and RE_{Tw}). The dark shaded blue color represents the threshold used to discriminate between wintry mixes containing SN vs those that did not.

supported by the developmental dataset which shows the chances for cases involving FZRA falling at a rate near 20% for each 1 J kg^{-1} drop in the ME_{Tw}.

Probabilities for PL can be determined in a similar manner. Assuming melting energy is nonzero, the chance of PL in the observation drops below 20% for $RE_{Tw} < 83 + 0.08ME_{Tw}$, where 83 J kg^{-1} is approximately the 20th percentile of RE_{Tw} from the distribution of wintry mixes with PL. Fitting this equation to the same logarithmic function in Eq. (5) results in the 20% threshold for PL in the observation to be $RE_{Tw} < 7 + 17.9\ln(ME_{Tw} + 1)$. This function along with Eq. (6a) is used to derive the probability of PL (ProbPL) as follows:

$$\text{ProbPL} = 2.3RE_{Tw} - 42\ln(ME_{Tw} + 1) + 3\,, \qquad (8)$$

with results constrained to values between 0 and 100.

As a final step, the ProbIce adjustment is applied to results of Eqs. (7) and (8). ProbFZRA is adjusted by multiplying by ProbIce/100, then adding (100 − ProbIce). ProbPL is scaled downward via multiplication by ProbIce/100. The final probabilities again are constrained between 0 and 100.

The process of deriving probabilities for FZRA and PL from the melting and refreezing energies, along with the presence of ice, does result in a rather wide zone of possible mixed precipitation forecasts, as illustrated in Fig. 5. However, as previously mentioned, this is desirable since mixes of the two precipitation types are routinely observed in nature. The transition zone also captures the difference between pure FZRA and PL events.

b. *Criteria for snow in wintry mixes*

Most precipitation type algorithms do not attempt to identify the potential of SN in wintry mixes, especially in cases featuring an elevated warm layer. Recall that this is the case with the original Bourgouin technique, where only a forecast for FZRA, PL, or a mix of the two is possible when the elevated warm layer has more than 2 J kg^{-1} (Bourgouin 2000). Given that SN can be observed as part of a wintry mix, we seek to determine the ME_{Tw} magnitudes favorable for such. Figure 4 indicates that for all the mixed precipitation cases in which SN was observed (rightmost two types in Fig. 4), the median ME_{Tw} values were near or just below 10 J kg^{-1}. This was in sharp contrast to cases void of SN, which were found to have significantly higher ME_{Tw} magnitudes. This suggests there is a threshold of ME_{Tw} that favors at least partial melting of all hydrometers, regardless of size.

Figures 6 and 7 display mixed precipitation cases with and without SN, respectively. These are similar to Fig. 5 but with the coordinates switched. In these figures, once ME_{Tw} exceeds 12 J kg^{-1} the number of cases with SN decreases significantly. In fact, 60% of the cases with SN occurred with ME_{Tw} at or below 12 J kg^{-1}, and 75% occurred with ME_{Tw} at or below 20 J kg^{-1}. This suggests that total melting of all hydrometers may not occur until ME_{Tw} exceeds 20 J kg^{-1}, which is higher than identified in Bourgouin (2000).

Interestingly, seven events had SN reported with ME_{Tw} in excess of 30 J kg^{-1}. Four of these had ME_{Tw} over 89 J kg^{-1}. It is unlikely that hydrometeors of any size would remain frozen with so much melting energy (Bourgouin 2000). We therefore explored the possibility this SN was generated in the cold surface layer and found the average RE_{Tw} in these cases to be 173 J kg^{-1}. This suggests these events had very cold and deep surface layers supportive of heterogeneous nucleation and SN generation in the cloud beneath the melting layer.

Given our goal is to identify a ME_{Tw} threshold to differentiate mixed precipitation events with SN from those without, the seven cases with surface-layer snow generation were removed from this analysis. Similarly, we removed the null snow cases that possessed ME_{Tw} in excess of 30 J kg^{-1}. This left a total of 30 mixed events with SN and 54 without.

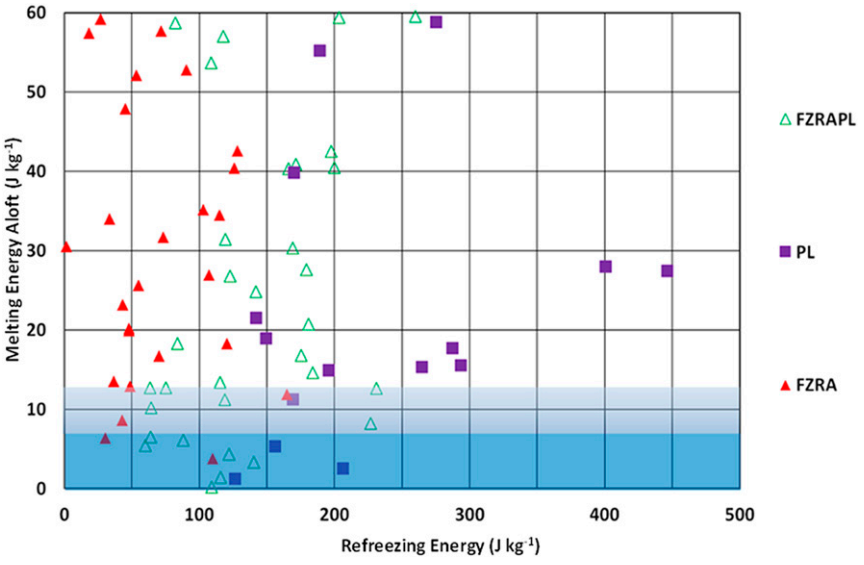

FIG. 7. As in Fig. 6, but for wintry mix cases not containing SN.

Figure 8 provides ME_{Tw} distributions for these two samples. While the two distributions do overlap, a Mann–Whitney *U*-test revealed that these distributions were significantly different above a 99% confidence level. This provides evidence that only weaker ME_{Tw} magnitudes would support the presence of snow.

The two ME_{Tw} distributions in Fig. 8 cross at approximately 9 J kg^{-1}. This occurs right around the highest and lowest 30th percentiles for cases with and without SN, respectively. As the ME_{Tw} exceeds 9 J kg^{-1} the ratio of percentiles for cases with SN to those void of SN begins to quickly fall below 1. The ratio drops at an exponential rate to below 0.2 at a ME_{Tw} of 15 J kg^{-1}. Using an exponential best fit for this drop in the ratios between the two datasets from a ME_{Tw} of 9 to 15 J kg^{-1} we derive the probability of SN (ProbSN) to be

$$\text{ProbSN} = 1540e^{-(0.29\text{ME}_{\text{Tw}})}, \tag{9}$$

with results limited to values between 0 and 100. Similar to the calculation for ProbPL, the final ProbSN value is obtained by multiplying the result of Eq. (8) by ProbIce/100.

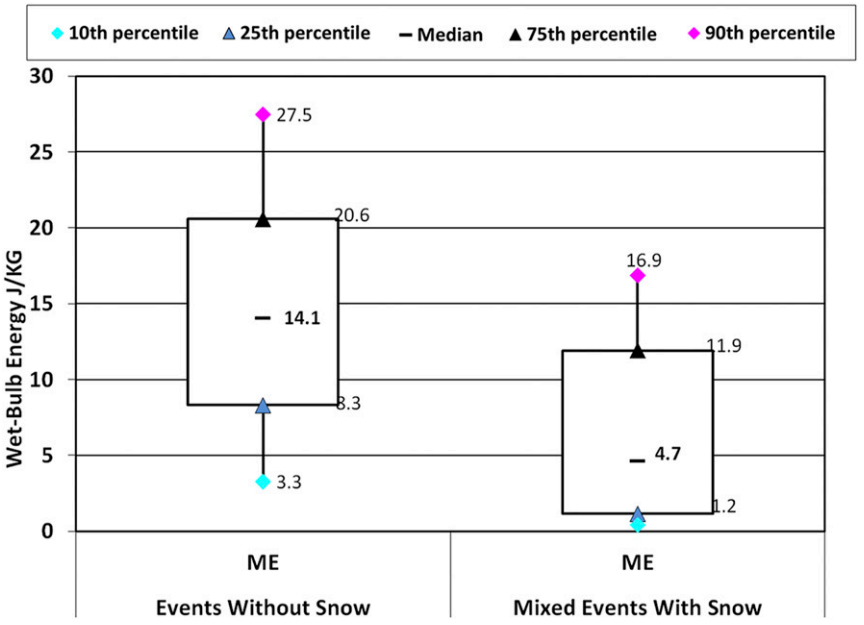

FIG. 8. Wet-bulb melting energies (ME_{Tw}) for wintry mixes that contained SN and those that did not. Cases with ME_{Tw} above 30 J kg^{-1} are excluded.

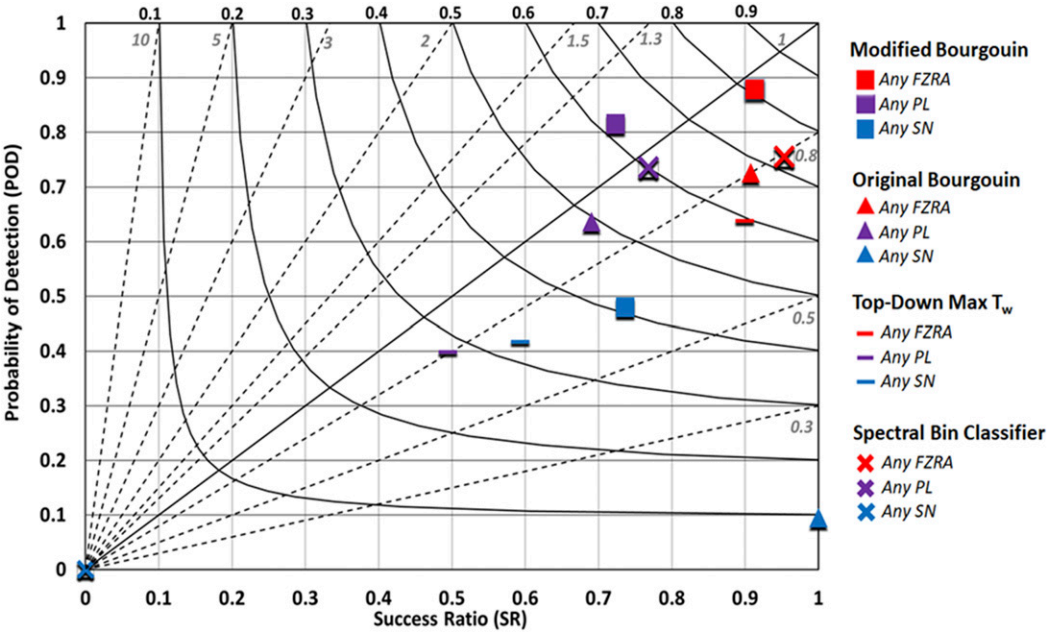

FIG. 9. Performance diagram for four precipitation-type methods: Modified Bourgouin (squares), original Bourgouin (triangles), MaxTwAloft (dashes), and spectral bin classifier (X marks). Forecast comparisons are for any FZRA (red), PL (purple), and SN (blue) in the observation. Curved lines represent the critical success index (CSI) while the diagonal lines represent bias.

While Eq. (9) was derived from cases involving a melting layer aloft, it can also be used to diagnose the potential for SN in environments with a melting layer near the surface. We tested Eq. (9) on 44 such cases and obtained a POD for SN of 0.86. This was in comparison to a POD of 0.57 using the original Bourgouin.

The appendix contains a summary of the steps involved in calculating probabilities for all four precipitation types.

5. Performance of the modified technique

This section evaluates the Modified technique's performance using the independent dataset. We also compare its performance to that of the original Bourgouin area method, the SBC, and the traditional top-down methodology that utilizes MaxTwAloft. First we examine how well these algorithms predict FZRA and PL either alone or as part of a mix, and also how they predict SN as part of a mix. Then we see how closely their predictions match the full observations. For example, when only FZRA is reported we desire a forecast of FZRA alone, not a FZRAPL mix. Or when FZRAPL is reported we want only FZRAPL in the forecast.

This second, more stringent, evaluation is motivated by the way these forecasts can be utilized operationally, especially when QPF is derived independently of precipitation type. In that situation, the total QPF is distributed between different precipitation types according to the probability of each type. For example, if the algorithm yields a 100% chance of SN, all of the QPF would be assigned to SN. If, however, there was also a 30% chance of PL, then 77% (100/130) would go to SN and 23% (30/130) would go to PL. It is not desirable to split QPF in this way if only one type is actually occurring. The purpose of this more stringent test is to evaluate how well the algorithms predict all precipitation types in the observation.

Note that with this approach, a 50%/50% mix is equivalent to a 100%/100% mix. So there could be a forecast of 100% PL and 100% FZRA derived from Fig. 5. Or there could be a forecast of 100% PL that becomes a forecast of 50% PL and 50% FZRA after the ProbIce adjustment is applied. Both forecasts are equivalent for this evaluation.

The independent dataset for this study consists of 172 events from 2006 to 2019. Table 1 shows the number of cases for each precipitation type. While a larger dataset would lend greater confidence to these results, we seek a preliminary sense of how the different methodologies compare. This also is a far larger independent dataset than used in the original Bourgouin (2000) study.

For the first evaluation, the performance diagram in Fig. 9 allows for direct comparison of the different techniques by displaying four verification statistics: the probability of detection (POD), success ratio (SR, or 1 − false alarm ratio), bias, and critical success index (CSI) as described in Roebber (2009). The focus here is on any cases involving FZRA or PL either alone or as part of a mix, and SN as part of a mix.

Recall that the SBC and original Bourgouin methods are deterministic and provide a simple "yes" forecast of the one precipitation type or mix deemed most likely. In contrast, the traditional top-down and Modified Bourgouin techniques forecast the probability of four different types (RA, SN, PL, and FZRA) from which the probability of mixes also can be

TABLE 2. Heidke skill score (HSS) for any FZRA, PL, and SN in the observation from the traditional top-down max T_w, original Bourgouin, the Modified Bourgouin, and the Reeves SBC. The largest HSS for each type is shown in bold italics.

HSS	FZRA	PL	SN
Top-down max T_w	0.27	0.11	0.36
Original Bourgouin	0.36	0.42	0.11
Modified Bourgouin	***0.55***	***0.58***	***0.48***
Reeves SBC	0.49	0.56	0.00

inferred. Consider a hypothetical scenario where the probabilistic output gives 60% for FZRA, 40% for PL and 30% for SN. If the actual observation is FZRAPL, then for Fig. 9 there would be a 0.6 hit for FZRA, a 0.4 hit for PL, and a 0.3 false alarm for SN.

In Fig. 9, a point nearer the center diagonal and upper-right corner shows less forecast bias (between POD and SR) and greater skill (CSI) than a point farther away. For FZRA, and for SN as part of a mix, the Modified Bourgouin technique produced the largest CSI of the four methods. Note that the SBC does not forecast SN when there is an elevated melting layer, and the MaxTwAloft method only does so when that layer is extremely small.

The clustering of PL scores at a lower CSI suggests this is a more difficult forecast for all the methods, and that all but the MaxTwAloft approach handle it similarly. Forecast skill for PL was very similar for the Modified Bourgouin technique and the SBC.

An important takeaway from Fig. 9 is the considerable improvement of the Modified Bourgouin method over the original. For FZRA the higher POD with little change in the bias is especially important given the considerable impacts associated with such events. This likely is due in part to the inclusion of a ProbIce check. In the independent dataset there were 31 FZRA cases with ProbIce ≤ 50. For these events the Modified Bourgouin POD was 0.96 while POD for the original was only 0.60. Similarly, when testing Eq. (7) on 60 FZDZ cases we obtained a POD of 0.92 with a CSI of 0.79. Moreover, the notable improvement to the Heidke skill score (HSS) for FZRA shown in Table 2 also indicates better forecasts of null events.

The diagram in Fig. 10 is similar to Fig. 9; however, the focus here is how well each algorithm exactly matches the observations. The performance for cases of FZRA and PL thus represent only those in which they were the sole precipitation type observed. Results for the various winter mixes involving the occurrences of FZRA and PL together (FZRAPL), and with SN (FZRAPLSN and PLSN), also are displayed.

When evaluating the skill at forecasting only a desired type or mix, the two probabilistic algorithms are penalized for including nonzero probabilities of undesired types. Specifically,

$$\text{PureProb} = \frac{\text{DesiredProb} - \max(\text{UndesiredProbs})}{\max(\text{AllProbs})}, \quad (10)$$

$$\text{PureMixProb} = \frac{\min(\text{DesiredProbs}) - \max(\text{UndesiredProbs})}{\max(\text{AllProbs})}, \quad (11)$$

where PureProb and PureMixProb represent the probability of having *only* the desired type or mix, DesiredProb(s) represents the probability of the desired type(s), UndesiredProbs represents the probabilities of each type not desired, and AllProbs represents the probability for all four types. In

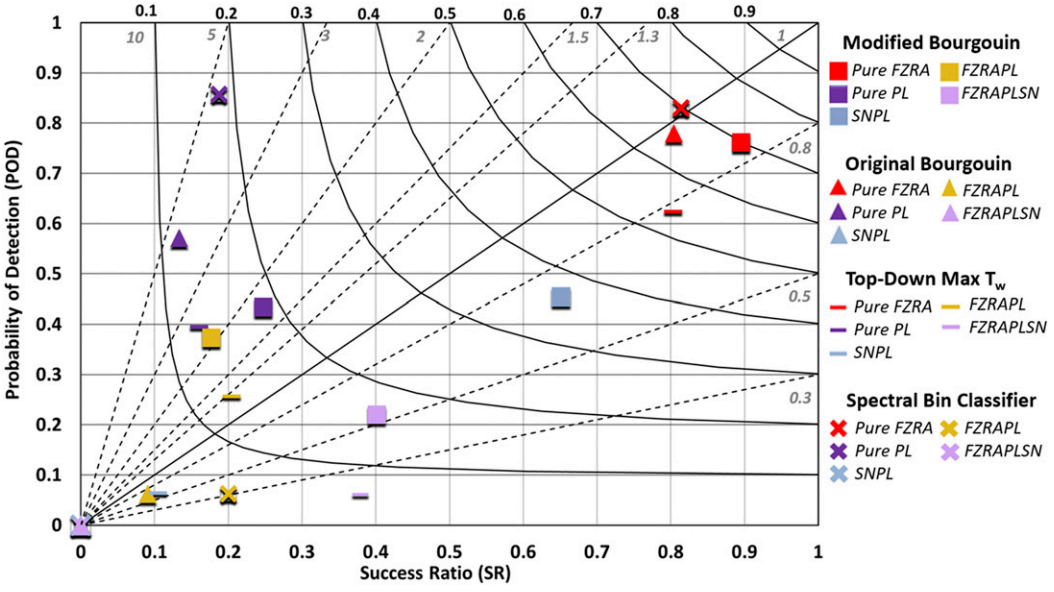

FIG. 10. As in Fig. 9, but for forecast comparisons for FZRA (red), PL (purple), FZRAPL (yellow), FZRAPLSN (light purple), and PLSN (light blue) for four precipitation-type methods: Modified Bourgouin (squares), original Bourgouin (triangles), MaxTwAloft (dashes), and spectral bin classifier (X marks).

TABLE 3. Critical success index (CSI) and the Heidke skill score (HSS) for events of pure FZRA, pure PL, mixes of the two (FZRAPL), and for all combined precipitation types. The largest CSI and HSS for each type are shown in bold italics.

CSI/HSS	FZRA	PLSN	PL	FZRAPL	FZRAPLSN	All types
Top-down max T_w	0.54/0.35	0.04/-0.03	0.13/0.12	0.13/***0.14***	0.06/0.08	0.30/0.34
Original Bourgouin	0.66/0.51	0.00/0.00	0.12/0.10	0.04/0.00	0.00/0.00	0.34/0.33
Modified Bourgouin	***0.70/0.62***	***0.37/0.48***	***0.19/0.24***	***0.14***/0.13	***0.17/0.22***	***0.43/0.50***
SBC	***0.70***/0.57	0.00/0.00	0.18/0.20	0.05/0.05	0.00/0.00	0.39/0.38

both equations the lower bound is zero so we avoid negative probabilities.

Using Eqs. (10) and (11) with the same hypothetical scenario as before, the PureFZRA probability would be 33% [(60 − 40)/60], PureFZRAPL would be 17% [(40 − 30)/60], and PureFZRAPLSN would be 50% [(30 − 0)/60]. If the observation is FZRAPL then FZRA and PL are the desired forecast types. For purposes of Fig. 10 this yields a POD of 0.17, a false alarm of 0.33 for pure FZRA, and a false alarm of 0.5 for FZRAPLSN. If the observation is PL this forecast receives no credit in Fig. 10 since FZRA had a higher probability.

Results in Fig. 10 indicate that the Modified Bourgouin technique continues to display improved skill at predicting pure FZRA events over the original Bourgouin method. Also noteworthy is its superior skill at predicting wintry mixed events (FZRAPL, FZRAPLSN and PLSN), while having no adverse impact on the performance for pure FZRA events. Overall, with the exception of pure PL events, the Modified Bourgouin technique produced superior skill and HSS values for all precipitation types (Table 3).

6. Summary and conclusions

The original Bourgouin technique (2000) is good at detecting FZRA events, but suffers from its inability to account for the potential lack of heterogeneous ice nucleation in the precipitation generation layer and evaporative cooling in unsaturated environments. The method also is hindered by its small developmental dataset. Therefore, in an effort to make the method a more viable precipitation type algorithm for operational forecasting, a modified version of the method was developed. This modified method is based on a much larger dataset, utilizes the wet-bulb profile instead of temperature, and incorporates a check for heterogeneous ice nucleation. New functions were empirically derived to discriminate between pure FZRA, wintry mixes, and pure PL. The modified method also allows for inclusion of SN despite an elevated melting layer. Together these changes yield significant performance improvements over the original Bourgouin and traditional top-down methods.

Because the Modified Bourgouin method was developed using observational data, it does not suffer from model bias and can be run with any numerical prediction model or with a blend of several models to produce gridded forecasts. While the revised method does not directly account for hydrometeor characteristics or the effects of precipitation rates, they are indirectly accounted for through the use of PoWTs. Preliminary verification results suggest its performance compares favorably to the more complex SBC that does attempt to account for hydrometeor characteristics. The Modified Bourgouin algorithm thus appears to show enough skill to be viable for NWP postprocessing, while also being simple enough to apply operationally for real-time forecast adjustments utilizing current observations.

An earlier version of the Modified Bourgouin technique was tested operationally at the NWS Weather Forecast Office (WFO) in Chicago for the winter of 2017–18, then as part of a larger testbed with over a dozen NWS WFOs during the 2018–19 and the 2019–20 winter seasons. Forecaster feedback has been positive. The earlier version also was adapted for versions 3.2 and 4.0 of the NWS National Blend of Models (NBM; Craven et al. 2018). The version of the Modified Bourgouin technique presented in this paper represents its latest iteration based on feedback from three anonymous reviewers and additional refinement by the authors.

Acknowledgments. The authors thank Dan Baumgardt, Andy Just, the NWS Central Region Forecast Builder team, and the NWS MDL for their assistance with this project, including adding the Modified Bourgouin algorithm into the NWS forecast tools (Forecast Builder) and adapting it for the NBM. We also thank Jeff Manion, NWS Central Region Headquarters, for a detailed review of the text. Three anonymous reviewers provided valuable comments and suggestions, which were greatly appreciated.

Data availability statement. All upper air and surface observations used during this study are openly available from the National Centers for Environmental Information at https://www.ncei.noaa.gov/.

APPENDIX

Calculating the Probability of Each Weather Type

a. Calculating ProbSN

Step 1: $\text{ProbSN}_i = 1540e^{-(0.29\text{ME}_{\text{Tw}})}$.

ME_{Tw} is all wet-bulb melting energy in the atmospheric column. ProbSN_i is constrained between 0 and 100.

Step 2: $\text{ProbSN} = (\text{ProbIce}/100)\text{ProbSN}_i$.

ProbIce is the probability of ice presence in the precipitation generation layer. ProbSN is constrained between 0 and 100.

b. Calculating ProbPL (only when ME_{Tw} is nonzero)

Step 1: $\text{ProbPL}_i = 2.3\text{RE}_{\text{Tw}} - 42\ln(\text{ME}_{\text{Tw}} + 1) + 3$.

ME_{Tw} is the wet-bulb melting energy above a near-surface cold layer with nonzero RE_{Tw} (wet-bulb refreezing energy). $ProbPL_i$ is constrained between 0 and 100.

Step 2: ProbPL = (ProbIce/100)$ProbPL_i$.
ProbIce is the probability of ice presence in the precipitation generation layer. ProbPL is constrained between 0 and 100.

c. Calculating ProbFZRA or ProbRA

Step 1: $ProbFZRA_i = -2.1RE_{Tw} + 0.2ME_{Tw} + 458$.
ME_{Tw} is the wet-bulb melting energy. RE_{Tw} is the wet-bulb refreezing energy beneath any warm layers aloft. $ProbFZRA_i$ is constrained between 0 and 100.

Step 2: If ME_{Tw} is $< 5\,J\,kg^{-1}$: $ProbFZRA_i = ProbFZRA_i \times 0.2ME_{Tw}$.

Step 3: ProbFZRA = (100 − ProbIce) + (ProbIce/100)$ProbFZRA_i$.
ProbIce is the probability of ice presence in the precipitation generation layer. ProbFZRA constrained between 0 and 100. Where surface $T_w > 0$°C: ProbRA = ProbFZRA.

REFERENCES

Baldwin, M., R. Treadon, and S. Contorno, 1994: Precipitation type prediction using a decision tree approach with NMC's mesoscale eta model. Preprints, *10th Conf. on Numerical Weather Prediction*, Portland, OR, Amer. Meteor. Soc., 30–31.

Baumgardt, D., 2000: Precipitation type forecasting. Accessed 17 May 2020, http://rammb.cira.colostate.edu/training/visit/training_sessions/precipitation_type_forecasting/.

——, A. Just, and P. E. Shafer, 2017: Deriving precipitation type probabilities in the national blend of models. *28th Conf. on Weather Analysis and Forecasting/24th Conf. on Numerical Weather Prediction*, Seattle, WA, Amer. Meteor. Soc., 1190, https://ams.confex.com/ams/97Annual/webprogram/Paper313165.html.

Bernstein, B. C., 2000: Regional and local influences on freezing drizzle, freezing rain, and ice pellet events. *Wea. Forecasting*, **15**, 485–508, https://doi.org/10.1175/1520-0434(2000)015<0485:RALIOF>2.0.CO;2.

Bourgouin, P., 2000: A method to determine precipitation types. *Wea. Forecasting*, **15**, 583–592, https://doi.org/10.1175/1520-0434(2000)015<0583:AMTDPT>2.0.CO;2.

Changnon, S. A., 2003: Urban modification of freezing-rain events. *J. Appl. Meteor.*, **42**, 863–870, https://doi.org/10.1175/1520-0450(2003)042<0863:UMOFE>2.0.CO;2.

Cortinas, J. V., Jr., 2000: A climatology of freezing rain in the Great Lakes region of North America. *Mon. Wea. Rev.*, **128**, 3574–3588, https://doi.org/10.1175/1520-0493(2001)129<3574:ACOFRI>2.0.CO;2.

——, B. C. Bernstein, C. C. Robbins, and J. W. Strapp, 2004: An analysis of freezing rain, freezing drizzle, and ice pellets across the United States and Canada: 1976–1990. *Wea. Forecasting*, **19**, 377–390, https://doi.org/10.1175/1520-0434(2004)019<0377:AAOFRF>2.0.CO;2.

Craven, J. P., and Coauthors, 2018: Overview of National Blend of Models version 3.1. Part I: Capabilities and an outlook for future upgrades. *25th Conf. on Probability and Statistics*, Austin, TX, Amer. Meteor. Soc., 7.3, https://ams.confex.com/ams/98Annual/webprogram/Paper325347.html.

Crawford, R. W., and R. E. Stewart, 1995: Precipitation type characteristics at the surface in winter storms. *Cold Reg. Sci. Technol.*, **23**, 215–229, https://doi.org/10.1016/0165-232X(94)00014-O.

Czys, R., R. Scott, K. C. Tang, R. W. Przybylinski, and M. E. Sabones, 1996: A physically based, nondimensional parameter for discriminating between freezing rain and ice pellets. *Wea. Forecasting*, **11**, 591–598, https://doi.org/10.1175/1520-0434(1996)011<0591:APBNPF>2.0.CO;2.

Glahn, H. R., and D. P. Ruth, 2003: The new digital forecast database of the National Weather Service. *Bull. Amer. Meteor. Soc.*, **84**, 195–202, https://doi.org/10.1175/BAMS-84-2-195.

Klein, W. H., B. M. Lewis, and I. Enger, 1959: Objective prediction of five day mean temperature during winter. *J. Meteor.*, **16**, 672–682, https://doi.org/10.1175/1520-0469(1959)016<0672:OPOFDM>2.0.CO;2.

Landolt, S. D., J. S. Lave, D. Jacobson, A. Gaydos, S. DiVito, and D. Porter, 2019: The impacts of automation on present weather-type observing capabilities across the conterminous United States. *J. Appl. Meteor. Climatol.*, **58**, 2699–2715, https://doi.org/10.1175/JAMC-D-19-0170.1.

Mahoney, E. A., and T. A. Niziol, 1997: BUFKIT: A software application toolkit for predicting lake-effect snow. Preprints, *13th Int. Conf. on Interactive Information and Processing Systems for Meteorology, Oceanography, and Hydrology*, Long Beach, CA, Amer. Meteor. Soc., 388–391.

Manikin, G. S., 2005: An overview of precipitation type forecasting using NAM and SREF data. Preprints, *21st Conf. on Weather Analysis and Forecasting/17th Conf. on Numerical Weather Prediction*, Washington, DC, Amer. Meteor. Soc., 8A.6, https://ams.confex.com/ams/pdfpapers/94838.pdf.

Mullens, E. D., and R. McPherson, 2017: A multialgorithm reanalysis-based freezing-precipitation dataset for climate studies in the south-central United States. *J. Appl. Meteor. Climatol.*, **56**, 495–517, https://doi.org/10.1175/JAMC-D-16-0180.1.

Pobanz, B. M., J. D. Marwitz, and M. K. Politovich, 1994: Conditions associated with large-drop regions. *J. Appl. Meteor. Climatol.*, **33**, 1366–1372, https://doi.org/10.1175/1520-0450(1994)033<1366:CAWLDR>2.0.CO;2.

Politovich, M., 1996: Response of a research aircraft to icing and evaluation of severity indices. *J. Aircr.*, **33**, 291–297, https://doi.org/10.2514/3.46936.

Ralph, F. M., and Coauthors, 2005: Improving short-term (0–48 h) cool-season quantitative precipitation forecasting: Recommendations from a USWRP workshop. *Bull. Amer. Meteor. Soc.*, **86**, 1619–1632, https://doi.org/10.1175/BAMS-86-11-1619.

Ramer, J., 1993: An empirical technique for diagnosing precipitation type from model output. Preprints, *Fifth Int. Conf. on Aviation Weather Systems*, Vienna, VA, Amer. Meteor. Soc., 227–230.

Rasmussen, R. M., I. Geresdi, G. Thompson, K. Manning, and E. Karplus, 2002: Freezing drizzle formation in stably stratified layer clouds: The role of radiative cooling of cloud droplets, cloud condensation nuclei, and ice initiation. *J. Atmos. Sci.*, **59**, 837–860, https://doi.org/10.1175/1520-0469(2002)059<0837:FDFISS>2.0.CO;2.

Rauber, R. M., L. S. Olthoff, and M. K. Ramamurthy, 2000: The relative importance of warm rain and melting processes in freezing precipitation events. *J. Appl. Meteor.*, **39**, 1185–1195, https://doi.org/10.1175/1520-0450(2000)039<1185:TRIOWR>2.0.CO;2.

——, ——, ——, and K. E. Kunkel, 2001: Further investigation of a physically based, nondimensional parameter for discriminating between locations of freezing rain and ice pellets. *Wea. Forecasting*, **16**, 185–191, https://doi.org/10.1175/1520-0434(2001)016<0185:FIOAPB>2.0.CO;2.

Reeves, H. D., K. L. Elmore, A. Ryzhkov, T. Schuur, and J. Krause, 2014: Sources of uncertainty in precipitation-type forecasting. *Wea. Forecasting*, **29**, 936–953, https://doi.org/10.1175/WAF-D-14-00007.1.

——, A. V. Ryzhkov, and J. Krause, 2016: Discrimination between winter precipitation types based on spectral-bin microphysical modeling. *J. Appl. Meteor. Climatol.*, **55**, 1747–1761, https://doi.org/10.1175/JAMC-D-16-0044.1.

Robbins, C. C., and J. V. Cortinas Jr., 2002: Local and synoptic environments associated with freezing rain in the contiguous United States. *Wea. Forecasting*, **17**, 47–65, https://doi.org/10.1175/1520-0434(2002)017<0047:LASEAW>2.0.CO;2.

Roebber, P., 2009: Visualizing multiple measures of forecast quality. *Wea. Forecasting*, **24**, 601–608, https://doi.org/10.1175/2008WAF2222159.1.

Schichtel, M., 1988: Specification of precipitation type in Oklahoma winter storms. M.S. thesis, Department of Meteorology, School of Meteorology, University of Oklahoma, 131 pp.

Schuur, T. J., H.-S. Park, A. V. Ryzhkov, and H. D. Reeves, 2012: Classification of precipitation types during transitional winter weather using the RUC model and polarimetric radar retrievals. *J. Appl. Meteor. Climatol.*, **51**, 763–779, https://doi.org/10.1175/JAMC-D-11-091.1.

Thériault, J. M., R. E. Stewart, and W. Henson, 2010: On the dependence of winter precipitation types and temperature, precipitation rate, and associated features. *J. Appl. Meteor. Climatol.*, **49**, 1429–1442, https://doi.org/10.1175/2010JAMC2321.1.

Wandishin, M. S., M. E. Baldwin, S. L. Mullen, and J. V. Cortinas Jr., 2005: Short-range ensemble forecasts of precipitation type. *Wea. Forecasting*, **20**, 609–626, https://doi.org/10.1175/WAF871.1.

Zerr, R. J., 1997: Freezing rain: An observational and theoretical study. *J. Appl. Meteor.*, **36**, 1647–1661, https://doi.org/10.1175/1520-0450(1997)036<1647:FRAOAT>2.0.CO;2.